Spontaneous Activity of Dopaminergic Retinal Neurons

Michael A. Steffen,* Christina A. Seay,* Behrang Amini,* Yidao Cai,* Andreas Feigenspan,† Douglas A. Baxter,* and David W. Marshak*

*Department of Neurobiology and Anatomy, University of Texas Medical School, Houston, Texas 77225 USA; and †Department of Neurobiology, University of Oldenburg, 26111 Oldenburg, Germany

ABSTRACT Dopaminergic local circuit neurons in the retina (DA cells) show robust, spontaneous, tetrodotoxin-sensitive pacemaking. To investigate the mechanism underlying this behavior, we characterized the sodium current and a subset of the potassium currents in the cells in voltage-clamp experiments. We found that there is a persistent component of the sodium current in DA cells which activates at more depolarized potentials than the transient component of the current. The transient component was completely inactivated at −50 mV, but DA cells remained able to fire spontaneous action potentials when potassium channels were partially blocked and the membrane potential remained above −40 mV. Based on these electrophysiological data, we developed a reduced computer model that reproduced the major features of DA cells. In simulations at the physiological resting potential, the persistent component of the sodium current was both necessary and sufficient to account for spontaneous activity, and the major contribution of the transient component of the sodium current was to initiate the depolarization of the model cell during the interspike interval. When tonic inhibition was simulated by lowering the input impedance of the model cell, the transient component played a larger role.

INTRODUCTION

Dopaminergic local circuit neurons in the retina (DA cells) play a critical role in visual adaptation. Dopamine acts on virtually all types of neurons in the retina, enabling them to remain sensitive to contrast as the intensity of the background light varies (reviewed by Li and Dowling, 2000). The finding that γ-aminobutyric acid (GABA) antagonists stimulate dopamine release suggested that DA cells are spontaneously active (Kamp and Morgan, 1981; Marshburn and Iuvone, 1981; O'Connor et al., 1986). Recently, this has been demonstrated directly in DA cells isolated from the mouse retina using whole-cell voltage- and current-clamp techniques (Feigenspan et al., 1998; Gustincich et al., 1997). There is also evidence that in vivo, the DA cells are spontaneously active in total darkness and enhance the sensitivity of the rod pathway under these conditions (Feigenspan et al., 1998; Marshak, 2001).

The mechanism underlying the spontaneous activity of retinal DA cells is quite different from that of midbrain DA cells. In midbrain DA cells, the spontaneous spiking is mediated by an L-type voltage-dependent calcium current (I_{Ca}) and an SK-type calcium activated potassium current (I_{KCa}) (reviewed by Wolfart et al., 2001). A hyperpolarization activated cation current (I_h) also plays a role in some midbrain DA cells (Seutin et al., 2001). However, the spontaneous activity in mouse retinal DA cells persists even after I_h is blocked by the application of extracellular cesium, after all calcium in the extracellular solution is replaced by cobalt, and when A- and D-type potassium channels are blocked with 4-aminopyridine (4-AP) (Feigenspan et al., 1998). Blockade of sodium channels with tetrodotoxin (TTX) completely eliminates both the action potentials and the subthreshold oscillations in the membrane potential (Feigenspan et al., 1998). DA cells have high-threshold calcium channels and hyperpolarization-activated cation channels, as well as three types of potassium channels: a calcium-activated potassium current, a tetraethylammonium (TEA)-sensitive current, and a 4-AP–sensitive current. All of these channels influence the shape and frequency of action potentials, but only the sodium currents and a small proportion of the potassium currents are necessary to generate spontaneous activity (Feigenspan et al., 1998; Gustincich et al., 1997).

The goal of the present study was to investigate the mechanisms underlying spontaneous activity in DA cells. Although a previous study did not distinguish different components of the sodium current in DA cells (Feigenspan et al., 1998), the voltage-clamp experiments described here suggest that there is a persistent component of the sodium current that activates at a more depolarized potential than the transient component of the current. Moreover, the spontaneous activity at relatively depolarized membrane potentials suggests that the persistent component of the sodium current plays a major role in generating the action potentials of the DA cell.

To better characterize the mechanism underlying the DA cell's behavior, we built a reduced computer model of the cell based on our electrophysiological data. We were able to fit the experimental results and simulate the spontaneous firing of isolated mouse DA cells. We found that the persistent component of the sodium current is necessary and sufficient to account for the spontaneous activity of the model DA cells. The model predicts that the most important

Submitted March 26, 2003, and accepted for publication June 16, 2003.

Address reprint requests to David W. Marshak, PhD, Dept. of Neurobiology and Anatomy, University of Texas Medical School, Houston, TX 77225 USA. Tel.: 713-500-5617; Fax: 713-500-0621; E-mail: david.w.marshak@uth.tmc.edu.

0006-3495/03/10/2158/12 $2.00

contribution of the transient component is to speed up depolarization of the DA cell during the interspike interval. Some of these results were presented previously in abstract form (Feigenspan et al., 2001).

METHODS

Electrophysiology

The electrophysiological methods used have been reported in earlier papers, and some of the voltage-clamp studies that we used as the basis of our modeling have been described elsewhere (Feigenspan et al., 2001; Feigenspan et al., 1998; Gustincich et al., 1997). Briefly, using a line of transgenic animals in which dopaminergic neurons express human placental alkaline phosphatase on the outer surface of their membranes, solitary dopaminergic neurons were identified in dissociated adult mouse retinas by labeling their membranes with a monoclonal antibody to human placental alkaline phosphatase (E6) conjugated to the fluorochrome Cy3. Patch-clamp recordings in the voltage-clamp mode were performed with an Axopatch 200A amplifier (Axon Instruments, Union City, CA). Currents were low-pass filtered using the internal Bessel filter of the amplifier, and the output was digitized with a DigiData 1200 interface (Axon Instruments) at sample frequencies of 10–50 kHz. Patch pipettes were constructed from borosilicate glass (1.65 mm o.d.,1.2 mm i.d.) using a horizontal two-stage electrode puller. The electrode resistance ranged from 5 to 7 MΩ; the series resistance of the pipettes was in the range of 10–20 MΩ and could be compensated up to 80% after cancellation of the capacitive transients. Drugs were applied to single cells in the extracellular solution by gravity flow through an array of microcapillary tubes connected to a Y tube. This application system allowed for a complete solution exchange in the vicinity of the recorded cell within 200–500 ms.

In voltage-clamp experiments to isolate the sodium current, the extracellular solution contained (in mM):100 NaCl, 60 TEACl, 2 $CaCl_2$, 0.3 $CdCl_2$, and 10 HEPES, and the intracellular solution contained (in mM): 120 CsCl, 20 TEACl, 1 $CaCl_2$, 2 $MgCl_2$, 11 EGTA, and 10 HEPES. In voltage-clamp experiments to isolate the 4-AP–insensitive component of the potassium current, the extracellular solution contained (in mM): 137 NaCl, 5.4 KCl, 1.8 $CaCl_2$, 1 $MgCl_2$, 5 HEPES, 1 μM TTX, and 4 mM 4-AP; and the intracellular solution contained (in mM): 140 KCl, 1 $CaCl_2$, 2 $MgCl_2$, 11 EGTA, and 10 HEPES. In current-clamp experiments, the extracellular solution contained (in mM): 137 NaCl, 5.4 KCl, 1.8 $CaCl_2$, 1 $MgCl_2$, 5 HEPES, 10 glucose. In experiments to study the effects of partial blockade of potassium channels, 40mM TEACl was substituted for NaCl. The intracellular solution contained (in mM): 125 K-gluconate, 10 KCl, 0.5 EGTA, and 10 HEPES. The pH of all solutions was adjusted with NaOH. All data were collected at room temperature.

Simulations

Simulations were performed on both Windows NT and Apple Macintosh computers with SNNAP (Simulator for Neural Networks and Action Potentials), version 5.1 (Ziv et al., 1994; snnap.uth.tmc.edu). The forward Euler method with a fixed time step of 5 μs was used for numerical integration. Curve fitting was done on an Apple Macintosh using QuantumSoft Pro Fit, version 5.1 (Uetikon am See, Switzerland).

Data preparation and general model features

Cells used in the voltage-clamp studies were assumed to have similar membrane properties. Therefore, differences in the membrane capacitance recorded in the study were attributed to differences in cell surface area, and the voltage-clamp data were normalized based on membrane capacitance. The current records were then averaged, and these average traces were used to generate the values of the parameters in the model. This preprocessing was done using custom Perl 5 scripts on an Intel-based microcomputer running Red Hat Linux. Since electrophysiological data were collected at room temperature, the model was constructed to replicate behavior at this temperature. Because the experiments were done using acutely isolated DA cells with short processes, the model simulates only the perikarya of DA cells.

The ionic currents in the model were described by standard, Hodgkin-Huxley–type equations in which generalized Boltzmann-type equations defined the voltage- and time-dependent activation and inactivation of conductances. Specifically, channel conductances were evaluated by solving the general equation:

$$g_{\text{ion}} = g_{\max(\text{ion})} A_{\text{ion}}^{\text{p}}(V_{\text{m}}, t) B_{\text{ion}}(V_{\text{m}}, t), \tag{1}$$

where $g_{\max(\text{ion})}$ is the maximal value of g_{ion}, $A_{\text{ion}}(V_{\text{m}},t)$ and $B_{\text{ion}}(V_{\text{m}},t)$ are functions describing the voltage and time dependence of activation and inactivation associated with g_{ion}, and p is the power to which A_{ion} was raised and was taken as the standard value for a given ion type. A_{ion} and B_{ion} were given by the solution to the general differential equations:

$$\frac{dA_{\text{ion}}}{dt} = \frac{A_{\infty(\text{ion})} - A_{\text{ion}}}{\tau_{\text{A(ion)}}} \tag{2a}$$

$$\frac{dB_{\text{ion}}}{dt} = \frac{B_{\infty(\text{ion})} - B_{\text{ion}}}{\tau_{\text{B(ion)}}}, \tag{2b}$$

where $A_{\infty(\text{ion})}$ and $B_{\infty(\text{ion})}$ are the voltage-dependent, steady-state values of the activation and inactivation functions, respectively; and $\tau_{\text{A(ion)}}$ and $\tau_{\text{B(ion)}}$ are the voltage-dependent time constants of the activation and inactivation functions, respectively. The values of $A_{\infty(\text{ion})}$ and $B_{\infty(\text{ion})}$ were determined from the general equations:

$$A_{\infty(\text{ion})} = \frac{1}{1 + \exp((V_{\text{m}} - h_{\text{A(ion)}})/s_{\text{A(ion)}})} \tag{3a}$$

$$B_{\infty(\text{ion})} = \frac{1}{1 + \exp((V_{\text{m}} - h_{\text{B(ion)}})/s_{\text{B(ion)}})}, \tag{3b}$$

where V_{m} is the membrane voltage, and $h_{\text{A(ion)}}$, $h_{\text{B(ion)}}$, $s_{\text{A(ion)}}$, and $s_{\text{B(ion)}}$ determine the midpoints and slopes of the steady-state activation and inactivation functions, respectively. When there was enough information to constrain the voltage dependence of the activation and inactivation time constants, they were represented by one of the two following functions. Otherwise, τ was held constant.

$$\tau = \frac{\tau_{\max} - \tau_{\min}}{1 + \exp((V_{\text{m}} - h_{1\tau(\text{ion})})/s_{1\tau(\text{ion})})} + \tau_{\min} \tag{4a}$$

$$\tau = \frac{\tau_{\max} - \tau_{\min}}{[1 + \exp((V - h_{1\tau(\text{ion})})/s_{1\tau(\text{ion})})][1 + \exp((V - h_{2\tau(\text{ion})})/s_{2\tau(\text{ion})})]} + \tau_{\min}, \tag{4b}$$

where V_{m} is the membrane voltage; $\tau_{\max}$ and $\tau_{\min}$ are the maximal and minimal values for the time constants, respectively; $h_{1\tau(\text{ion})}$, $h_{2\tau(\text{ion})}$, $s_{1\tau(\text{ion})}$, and $s_{2\tau(\text{ion})}$ determine the midpoints and slopes of the time constant functions, respectively. Equation 4a was used when the voltage dependence

of the time constant was best fit by a sigmoid in the physiological range, and Eq. 4b was used when the voltage dependence of the time constant was best fit by a Gaussian.

Determination of membrane parameters

The leak current in the cell was given a constant conductance of 0.4 nS based on the reported average input resistance of 2.4 GΩ (Feigenspan et al., 1998). Membrane capacitance was set at 8 pF, the average value recorded in the voltage-clamp study. Although the model is not geometric, this figure would correspond with a spherical soma of radius ~8 μm and membrane capacitance ~1 μF/cm^2, the typical value for cell membranes (Hille, 1992). This is consistent with the biological data; DA cells had perikarya that measured 14.7 μm in diameter, on average, and often had short processes attached (Gustincich et al., 1997; Feigenspan et al., 1998).

To fit voltage-clamp studies, the initial values of time constants and steady-state activation values for each test voltage were estimated and fit with generalized Boltzmann functions. The parameter values were then refined using a least-squares fit between the experimental data and the current calculated as a two-dimensional function of voltage and time, $I(V_m, t)$. Finally, minor adjustments were made to the parameter values, within the limits of the voltage-clamp data, to match the whole-cell simulations to the current-clamp records. In the voltage-clamp experiments to characterize the potassium currents, the initial ~2 ms of the traces were frequently obscured by residual sodium current and thus did not fully constrain the fits. Because the voltage-clamp experiments were carried out in low external sodium, the resulting reversal potential was substantially lower than in current-clamp recordings of spontaneous activity. To compensate for this difference, the reversal potential of sodium for the model was based on the current-clamp, rather than voltage-clamp, data. The reversal potential for potassium was calculated using the Nernst equation. Sodium currents were modeled with cubic activation functions and potassium currents were modeled with quartic activation functions (Hille, 1992). Because voltage-clamp data for the sodium and potassium channels were obtained from different cells, an accurate weighting of the two sets of currents could not be obtained from the voltage-clamp data alone. Consequently, the final conductance values of $I_{K,F}$ and $I_{K,S}$ were adjusted by hand in the final model to reproduce the current-clamp data.

RESULTS

Sodium currents

To characterize the voltage dependence and kinetics of the sodium currents in the DA cell, we stepped the membrane potential from −70 mV to more depolarized potentials with potassium and calcium channels blocked (Fig. 1 *A*). There were clearly transient and persistent components in the observed current, and both had reversal potentials of ~+25 mV. Because 300 μM cadmium was present to block the calcium currents, we concluded that both components of the current were carried by sodium ions. We measured the ratio of persistent current to peak current and found that it increased with depolarization (Fig. 1 *B*). The ratio of persistent to peak current reached its maximal value (0.38) at +35 mV, when both components of the current have reached full activation. This finding indicates that the persistent component of the sodium current activates at a more depolarized potential than the transient component.

To measure the voltage dependence of inactivation of the transient component of the sodium current, the DA cell was stepped to −30 mV from a wide range of holding potentials (Fig. 2, *A* and *B*). In all experiments with a holding potential positive of −50 mV, the transient component of the sodium current was completely absent. It had been shown previously that DA cells are able to generate spontaneous action potentials even when they are only able to repolarize partially (Feigenspan et al., 1998). When 40 mM TEA was applied to a spontaneously active DA cell to block most potassium currents, the DA cells continued to fire small, broad action potentials even though the membrane potential was always more positive than −40 mV. Fig. 2 *C* shows a modified version of Fig. 8 *A* from Feigenspan et al. (1998). Because spontaneous activity in DA cells is known to be completely blocked by TTX but persists when calcium channels are blocked (Feigenspan et al., 1998), we assumed that these spikes are mediated by sodium channels. However, because we had shown that the transient component of the sodium current never recovers from inactivation at these voltages, we hypothesized that the persistent component of the sodium current is sufficient to generate spontaneous activity in the DA cell. DA cells that are not spontaneously active have a resting membrane potential of −46 mV, on average (Feigenspan et al., 1998). This finding suggests that the persistent component of the sodium current plays a major role in generating the action potentials in the DA cells under normal conditions, as well.

Potassium currents

DA cells have an A-type potassium current that makes a major contribution to the resting membrane potential and

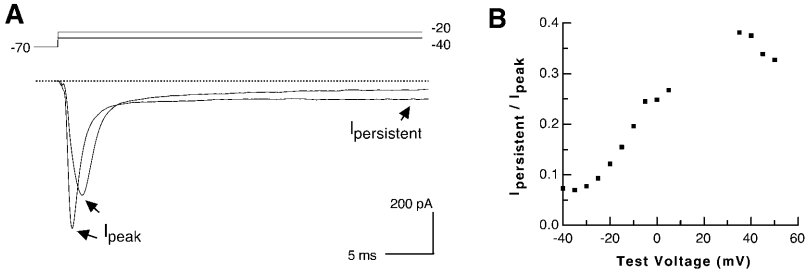

FIGURE 1 Voltage-clamp experiments demonstrating peak and persistent components of the sodium current. The membrane potential was stepped from −70 mV to more depolarized potentials under conditions designed to isolate the sodium current. (*A*) Averaged voltage-clamp traces of steps to −40 mV and −20 mV demonstrating peak and persistent components of the current. (*B*) The persistent component increases steadily as a fraction of peak current with increasing depolarization, until both peak and persistent current have reached full activation near +40 mV. Persistent current was defined as the average current measured between 40 and 45 ms after the onset of the voltage clamp. Data near +20 mV is not shown because this is near the reversal potential for sodium in the voltage-clamp experiments, and therefore both peak and persistent currents are very small.

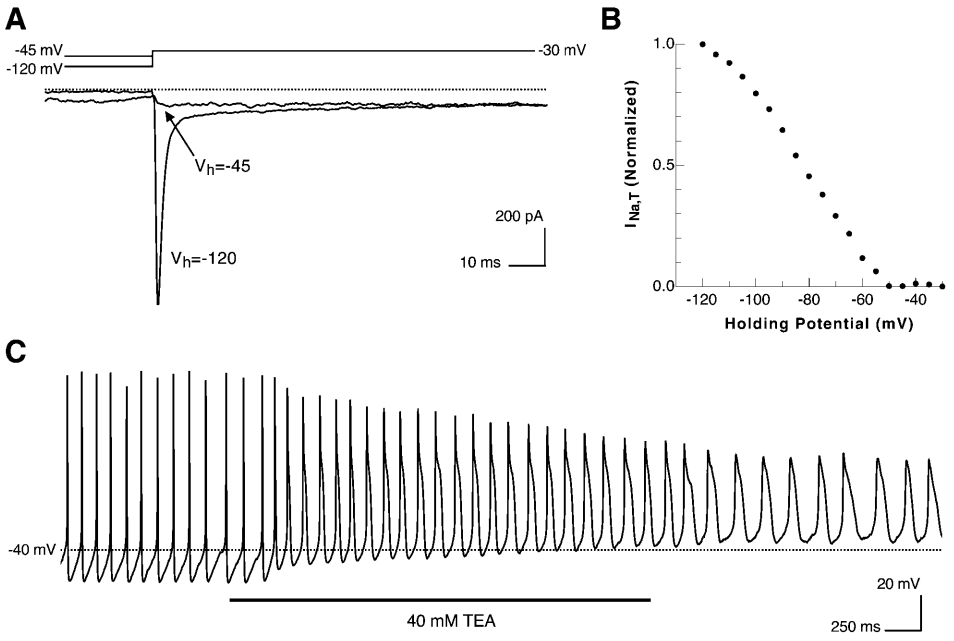

FIGURE 2 (*A*) Averaged voltage-clamp traces under conditions isolating the sodium current. In steps from −120 mV, there is a substantial transient component as well as a persistent component in the sodium current. Using a holding potential of −45 mV, the transient component is not detected. In both experiments, there was some steady-state current at the end of the step, which we attribute to the persistent component of the sodium current. (*B*) Transient current, measured as a fraction of the current measured in voltage-clamp experiments with a holding potential of −120 mV. The noninactivating current was subtracted out. The transient component of the sodium current has completely inactivated by steps to −45 mV. (*C*) Current-clamp recording of spontaneous activity in a DA cell. When a substantial fraction of the potassium channels is blocked with 40 mM TEA, the cell continues to fire small, broad action potentials, even though it is able to only partially repolarize. Modified from Fig. 8 *A* of Feigenspan et al. (1998).

the frequency of spontaneous firing; however, this current is not essential for spontaneous activity (Feigenspan et al., 1998). Because our primary interest was in the mechanism of spontaneous firing, we characterized the potassium current remaining after the A-type current was blocked with 4 mM 4-AP and the sodium current was blocked with 1 μm TTX. From a holding potential of −70 mV, the membrane was stepped to more depolarized potentials, beginning at −30 mV. The potassium current remaining after 4-AP blockade activated slowly and did not inactivate. Its activation was best fit by two time constants (Fig. 3 *A*). The fast and slow components of the potassium current differed primarily in their kinetics and amplitude; they had the same reversal potential and activated at similar voltages (Fig. 3 *B*). However, the slow component of the current appeared to have reached maximal conductance by +60 mV (the most depolarized voltage tested), whereas the conductance of the fast component of the current appeared to continue increasing at this voltage.

Model of the dopaminergic cell

To further explore the mechanism underlying the spontaneous activity in the DA cell, we built a reduced model of the cell based on the voltage-clamp data. The model included a conventional transient sodium conductance ($I_{Na,T}$), a noninactivating persistent sodium conductance ($I_{Na,P}$), two potassium conductances, and a leak current. We initially modeled the potassium current using a single current with two time constants, but a substantially better fit was obtained by modeling the data as two separate currents, $I_{K,F}$ (the ''fast'' potassium current) and $I_{K,S}$ (the ''slow'' potassium current). In addition, we later found that the inclusion of $I_{K,S}$ helped account for the depolarizing block

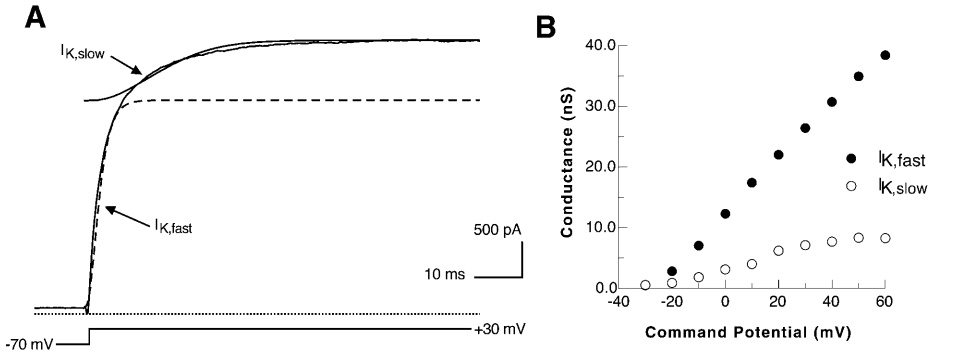

FIGURE 3 4-AP–resistant potassium current dynamics. (*A*) A typical voltage-clamp trace for the 4-AP–resistant K^+ current. It can be seen clearly that two time constants are necessary to model the activation of the current. With a two component model, a very good fit of simulation (*dashed line*) to experimental data (*solid line*) can be obtained. (*B*) Estimated voltage dependence of conductance for the fast and slow components of the potassium current.

in the model DA cell. Spontaneous activity persisted when only $I_{K,F}$ was present, however. Fig. 4 illustrates an equivalent circuit of the final model DA cell including all five conductances: $I_{K,F}$, $I_{K,S}$, $I_{Na,T}$, $I_{Na,P}$, and I_L. Fig. 5 shows the voltage dependence of each current in the model, as well as simulated voltage-clamp traces demonstrating fits to the experimental data.

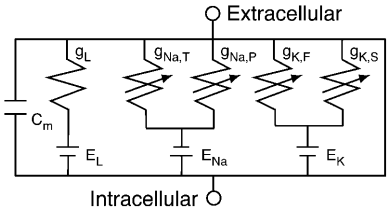

FIGURE 4 Equivalent electrical circuit of model DA cell membrane. Linear conductances are indicated by resistors and voltage-dependent conductances are indicated by variable resistors. Each conductance is associated with an equilibrium potential (E). In parallel with the membrane capacitance (C_M) are five ionic conductances: a leakage conductance (g_L); a transient Na^+ conductance ($g_{Na,T}$); a persistent Na^+ conductance ($g_{Na,P}$); a fast K^+ conductance ($g_{K,F}$); and a slow K^+ conductance ($g_{K,S}$).

Spontaneous activity of the model DA cell

The model cell was spontaneously active using the parameters listed in Table 1. The spontaneous activity was very robust under control conditions. We tested the cell at starting potentials ranging from −70 mV to +40 mV in 10 mV increments (Fig. 6). We also varied membrane capacitance, membrane resistance, and the ratio of Na^+ to K^+ currents by ±25%. In every case, the model DA cell spontaneously fired regular action potentials. Under control conditions, the cell reached +34 mV at the peak of each spike and hyperpolarized to −71 mV between spikes.

The properties of the spontaneous activity are listed and compared with those of dissociated DA cells from mouse retina in Table 2. The model DA cell was similar to the mouse DA cell in many respects. Although the observed spontaneous activity in the model cell varied in several ways from the mouse DA cells under control conditions, much of this variation likely can be explained by currents that are absent in our reduced model. The peak amplitude in the model DA cell is slightly lower than that in mouse DA cells under control conditions, which was +54 mV. This is likely due, in part, to the absence of calcium channels in the model DA cell. The peak amplitude of spikes in mouse DA cells was known to be reduced by 14% (~13 mV on average) when external calcium was replaced by cobalt to block the calcium current (Feigenspan et al., 1998). The model DA cell also fired at ~6 times the rate of mouse DA cells under control conditions. This increase in firing rate may be due, in part, to the absence of A-type and calcium-dependent potassium currents in the model DA cell; both types of potassium currents were known to reduce the firing rate of the mouse DA cells. When the A-type current was blocked with 4-AP in mouse DA cells, the interspike interval was reduced by 40%, and the spike amplitude was also reduced (Feigenspan et al., 1998). The action potentials were also broader in the model DA cell than in the mouse DA cells, and the afterhyperpolarization was somewhat more negative. Nevertheless, the reduced model reproduced the essential feature of the mouse DA cells, namely spontaneous activity that persists when calcium and most types of potassium channels are blocked (Feigenspan et al., 1998).

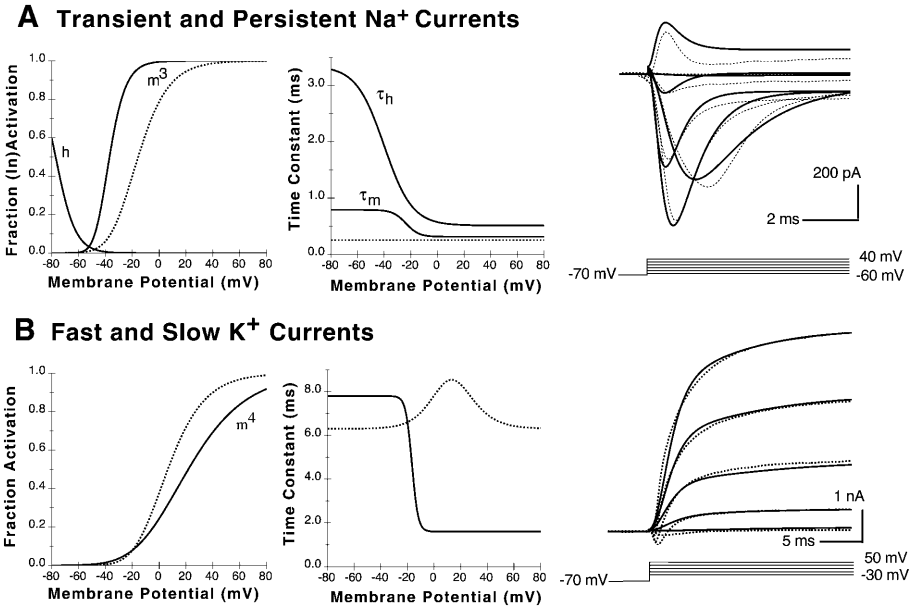

FIGURE 5 Activation and inactivation properties of the ionic conductances in the model. For each conductance, steady-state activation and inactivation are plotted against voltage at the left; the time constants of activation and inactivation are plotted in the middle; and a simulation of representative voltage-clamp currents are plotted on the right. In the third panel, the simulation is represented by the solid line and the averaged experimental data by the dotted line. (*A*) $I_{Na,T}$ (*solid lines*) and $I_{Na,P}$ (*dotted line*). (*B*) The two components of I_K. The fast component is shown with solid lines and the slow component with dashed lines. The voltage-clamp simulation includes both components together. There is a small, residual sodium current that obscures the initial few milliseconds in the experimental traces.

TABLE 1 Parameters describing membrane currents in control conditions

Current	E_r, mV	g_{max}, nS	h_A, mV	s_A, mV	p	$\tau_{A(max)}$, ms	$\tau_{A(min)}$, ms	$h_{\tau A1}$, mV	$s_{\tau A1}$, mV	$h_{\tau A2}$, mV	$s_{\tau A2}$, mV
Activation											
$I_{Na,T}$	80	270	−47	−7.3	3	0.79	0.31	−24	4.9		
$I_{Na,P}$	80	6.7	−34	−13.7	3	0.25					
$I_{K,F}$	−80	47	−23.6	−26.8	4	7.8	1.6	−16.6	2.3		
$I_{K,S}$	−80	9.5	−22	−17.1	4	15.4	6.3	10.9	11.6	11.4	−9.5
I_L	−50	0.4									

Current	h_B, mV	s_B, mV	$\tau_{B(max)}$, ms	$\tau_{B(min)}$, ms	$h_{\tau B}$, mV	$s_{\tau B}$, mV
Inactivation						
$I_{Na,T}$	−77	7.3	3.35	0.51	−40	10.5

E_r, reversal potential; g_{max}, maximal conductance; h_A, voltage parameter of activation function; s_A, slope parameter of activation function; p, power of activation function; $\tau_{A(max)}$, maximal activation time constant; $\tau_{A(min)}$, minimal activation time constant; $h_{\tau A1}$, first voltage parameter of activation time constant; $s_{\tau A1}$, first slope parameter of activation time constant; $h_{\tau A2}$, second voltage parameter of activation time constant; $s_{\tau A2}$, second slope parameter of activation time constant; h_B, voltage parameter of inactivation function; s_B, slope parameter of inactivation function; $\tau_{B(max)}$, maximal inactivation time constant; $\tau_{B(min)}$, minimal inactivation time constant; $h_{\tau B}$, voltage parameter for inactivation time constant; $s_{\tau B}$, slope parameter for inactivation time constant.

Role of the sodium current

As expected, the spontaneous activity of the model DA cell was sodium dependent. A complete block of the sodium channels was simulated by reducing the conductance of $I_{Na,P}$ and $I_{Na,T}$ to 0, and this eliminated spontaneous activity in the model DA cell. Under these conditions the model cell reached a steady resting voltage of −56 mV, a value similar to the average for mouse DA cells after TTX application, −50 mV (Feigenspan et al., 1998). As the experimental data suggest, the persistent component of the sodium current played a major role in spiking. When $I_{Na,P}$ was set to zero, the model DA cell was unable to fire spontaneous action potentials and reached a resting potential at −36mV (Fig. 7 *B*). It remains to be determined whether including additional potassium conductances would substantially affect this conclusion. However, when $I_{Na,T}$ was eliminated, the cell fired spontaneous action potentials similar to those under control conditions. The only major difference was in the spike frequency; without the transient current, the model DA cell fired at approximately one-third of its control rate (Fig. 7 *C*).

Analysis of the two sodium currents individually during spontaneous activity confirmed that $I_{Na,P}$ plays a dominant role in the model DA cell (Fig. 8). Whereas $I_{Na,T}$ was larger during the interspike interval and during the initial portion of the spike, I_{NaP} was substantially larger during most of the spike (Fig. 8 *A*). The total sodium current was quite small during the interspike interval (~1.5 pA at minimum), and $I_{Na,T}$ played its most significant role during this period (Fig. 8 *B*). Although $I_{Na,T}$ had a much greater maximal conductance as measured in the voltage-clamp experiments, only a very small portion could ever deinactivate under physiological conditions. Consequently, more current flowed through $I_{Na,P}$ except for a brief period during the interspike interval.

The model DA cell was also able to reproduce the spontaneous activity that persisted in mouse DA cells even when most potassium channels were blocked by 40 mM TEA. The application of TEA to the extracellular solution was simulated in the model DA cell by reducing each potassium conductance to 65% of its control value. Under these conditions, the model DA cell could only repolarize to −40 mV. However, the model cell still fired regular, small, broad spikes, with little change in frequency, as in mouse DA cells (Fig. 9 *A*). The role of I_{NaP} in spiking was even more pronounced (Fig. 9, *B* and *C*); $I_{Na,T}$ played a role only during the interspike interval. $I_{Na,T}$ could only recover from inactivation when the model DA cell was most hyperpolarized. Because $I_{Na,P}$ never inactivated, it was still able to maintain the spontaneous activity. These findings suggest

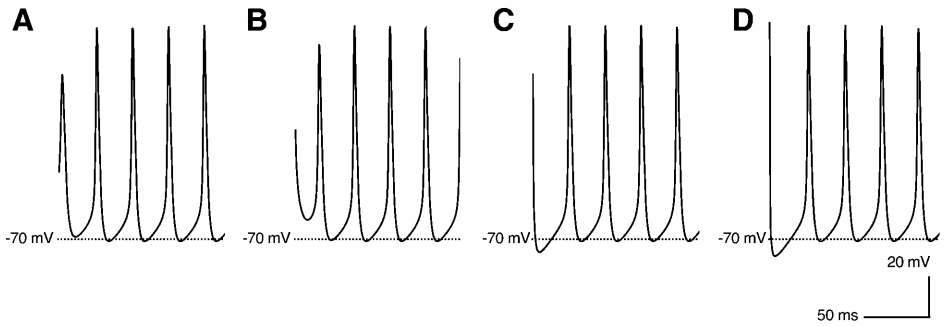

FIGURE 6 Spontaneous activity of the model DA cell at various starting membrane potentials. Behavior of the model cell under control conditions when it was started at (*A*) −40 mV, (*B*) −15 mV, (*C*) +10 mV, and (*D*) +35 mV. In every case, the cell fired at the same steady rate.

TABLE 2 Properties of spontaneous activity of model and mouse DA cells under control conditions

	Model	Mouse
Firing rate	36 Hz	6 Hz
Threshold	−54 mV	−37.8 mV
Peak amplitude above threshold	88 mV	91.5 mV
AHP peak below threshold	17 mV	11.08 mV
Width at threshold	6.4 msec	4.36 msec
Rise time (10%–90% threshold to peak)	1.5 msec	0.50 msec
Decay time (10%–90% peak to threshold)	2.5 msec	0.80 msec

Since the model cell is spontaneously active, the threshold is estimated by fitting the rising portion of a single spike with a sum of two exponential functions. The threshold is determined to be the voltage at which the rapidly rising exponential describing the spiking overtakes the slower exponential describing the interspike depolarization.

that the persistent component of the sodium current mediates spiking when the mouse DA cell is only able to repolarize to −40 mV. These spikes had amplitudes of 55 mV from trough to peak, the same as the smallest spikes observed in the mouse DA cells. The frequency of firing in the model differed substantially from that in the mouse DA cells, however. As before, a large part of the difference may be explained by the absence of the A-type and calcium-dependent potassium conductances in the model DA cell. This also may explain the sensitivity of the model DA cell to small changes in potassium current weights. In this reduced model, there was only a narrow range around 65% of the control values in which the small spikes are a steady-state behavior. When the weights were reduced by an additional 2%, the model DA cell reaches a resting potential −10 mV after a series of small spikes (Fig. 9 *D*). With weights of the potassium currents greater than 65% of control, the model fired a series of small spikes that gradually increased in amplitude until a steady state with larger spikes is reached (Fig. 9 *E*).

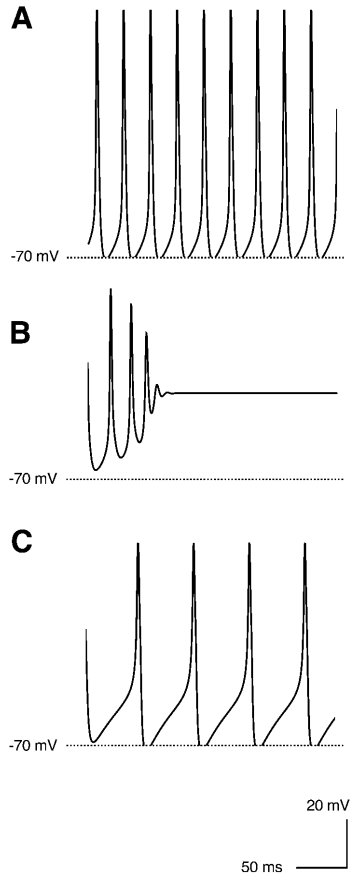

FIGURE 7 Role of the sodium current in spontaneous activity. (*A*) Simulated spontaneous activity in the full model; the starting membrane potential was −65 mV. Oscillations in membrane potential grew until a steady rate of firing was reached. (*B*) Simulation in the absence of $I_{Na,P}$; the starting membrane potential was −15 mV. Oscillations in membrane potential were dampened until the cell reached a steady resting potential at −35 mV. (*C*) Simulation in the absence of $I_{Na,T}$; the starting membrane potential was −15 mV. The cell fired spontaneous action potentials, but they were somewhat smaller and at a lower frequency than under control conditions.

Depolarizing block in the model DA cell

In mouse DA cells, the rate of spiking can be increased up to 22 Hz by depolarizing current, but depolarizing currents >20 pA produce a burst of 3–5 spikes followed by a depolarizing block (Feigenspan et al., 1998). In the original description of depolarizing block, the phenomenon was mediated by sodium inactivation (Hodgkin and Huxley, 1952). However, in the model DA cell, $I_{Na,P}$ does not inactivate and, therefore, sodium inactivation cannot account for the depolarizing block. Although $I_{K,S}$ was added to the model only to improve the fit to the experimental data, we later discovered that $I_{K,S}$ is able to produce a depolarizing block in the model DA cell (Fig. 10). During an injection of depolarizing current, $I_{K,S}$ was unable to follow the fluctuations in membrane potential and gradually grew larger. The increase in potassium current prevented the cell from depolarizing, and the membrane voltage enters a damped oscillation, eventually reaching a steady resting potential. This effect could be produced in the model cell with current injections of ≥85 pA. The fact that more current is required to generate depolarizing block in the model than in the mouse DA cells may be due to dynamic effects generated by unmodeled currents or to a slow inactivation process in the sodium current which we did not model.

Tonic inhibition in the model DA cell

Studies of dopamine release from the retina indicate that DA cells are under tonic, inhibitory control by GABAergic interneurons (Kamp and Morgan, 1981; Marshburn and Iuvone, 1981; O'Connor et al., 1986), and isolated DA cells have hyperpolarizing responses to GABA (Gustincich et al., 1997). Thus, the resting potential of DA cells in vivo may be

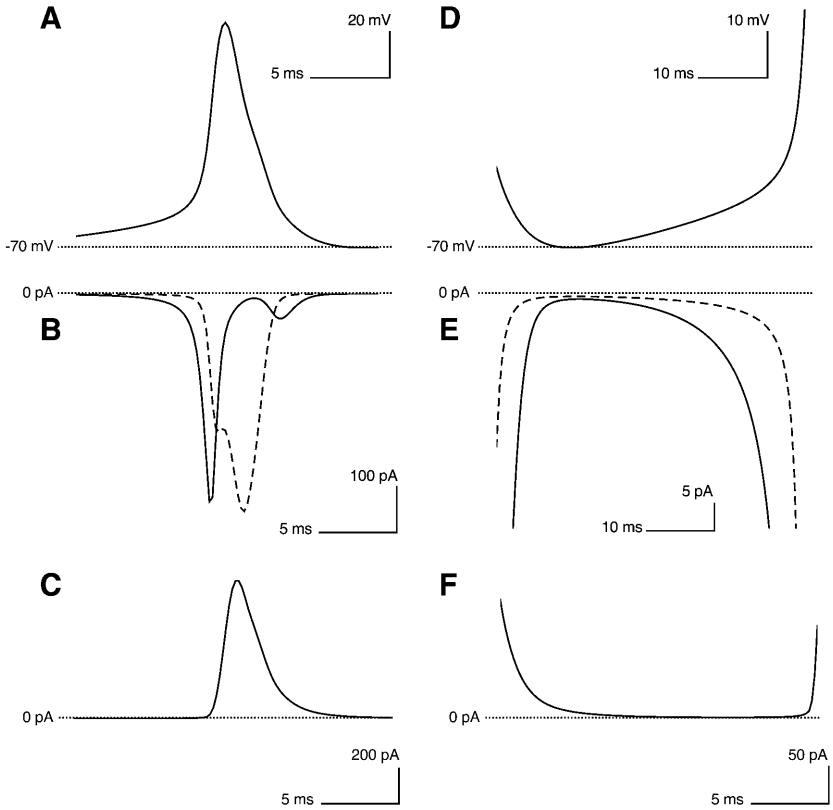

FIGURE 8 Contributions of the different components of the sodium current and the potassium currents to spontaneous activity. (*A*) A simulated action potential under control conditions. (*B*) Sodium currents during an action potential. $I_{Na,T}$ is represented by the solid line and $I_{Na,P}$ by the dashed line. Note that whereas $I_{Na,T}$ is dominant during the rising phase of the spike, $I_{Na,P}$ is the larger of the two during the remainder of the spike. (*C*) Total potassium current ($I_{K,F} + I_{K,S}$) during an action potential. $I_{K,F}$ and $I_{K,S}$ are shown together because under control conditions, the contribution of $I_{K,S}$ is very small and not significantly different from $I_{K,F}$. (*D*) The afterhyperpolarization and slow depolarization of the model cell during the interspike interval. (*E*) Sodium currents during the interspike interval. $I_{Na,T}$ is represented by the solid line and $I_{Na,P}$ by the dashed line. The total sodium current is quite small near the end of the spike (~1.5 pA at minimum). $I_{Na,T}$ plays a significant role during the interspike interval. (*F*) Total potassium current during the interspike interval.

more hyperpolarized than in isolated mouse DA cells, and the transient component of the sodium current would be expected to play a larger role than it does in vitro. To test this hypothesis using the model, we simulated the behavior of DA cells with a larger leak current that hyperpolarized the cell (Fig. 11). To examine the role of the persistent component in isolation, we used 2 nS; this was five times higher than the control value and the largest leak current that could be used and still generate multiple action potentials (Fig. 11 *A*). Under these conditions, there was only a single action potential, a finding suggesting that I_{NaT} played a far more important role. After the initial action potential, the model DA cell remained at −46 mV, the same resting potential, on average, observed in mouse DA cells that were not spontaneously active in the earlier experiments (Gustincich et al., 1997; Feigenspan et al., 1998). With both components of the sodium currents present in the model DA cells, it was possible to increase the leak current even further to 5 nS and still generate spontaneous action potentials. Under these conditions, I_{NaT} played a major role during the interspike interval and during the rising phase (Fig. 11, *B* and *C*).

DISCUSSION

In voltage-clamp experiments with DA cells under conditions designed to isolate sodium currents, we observed a transient component that was completely inactivated at −50 mV and a persistent component that apparently did not inactivate. Both components reversed at the same potential, and because 300 μm cadmium was present to block calcium channels, we concluded that the current was carried by sodium ions. This is consistent with previous reports that spontaneous subthreshold potentials and action potentials in DA cells are completely blocked by tetrodotoxin but insensitive to blockers of calcium and potassium channels (Gustincich et al., 1997; Feigenspan et al., 1998). DA cells are able to generate spontaneous action potentials when many of the potassium channels are blocked by 40 mM TEA and the membrane cannot repolarize beyond −40 mV (Feigenspan et al., 1998). Taken with the voltage-clamp data reported here, this finding suggests that the persistent component of the sodium current is sufficient to generate spontaneous action potentials in DA cells. However, further experiments would be required to confirm that the current generating these spikes is carried entirely by sodium ions.

The spontaneous action potentials in the DA cells arise from interactions between sodium and potassium currents, and they were clearly different from the oscillations produced by depolarizing current injection or applications of glutamate in a subset of teleost amacrine cells. The oscillations in the teleost amacrine cells arise from interactions between voltage-gated potassium currents and calcium currents, and they persist after the application of

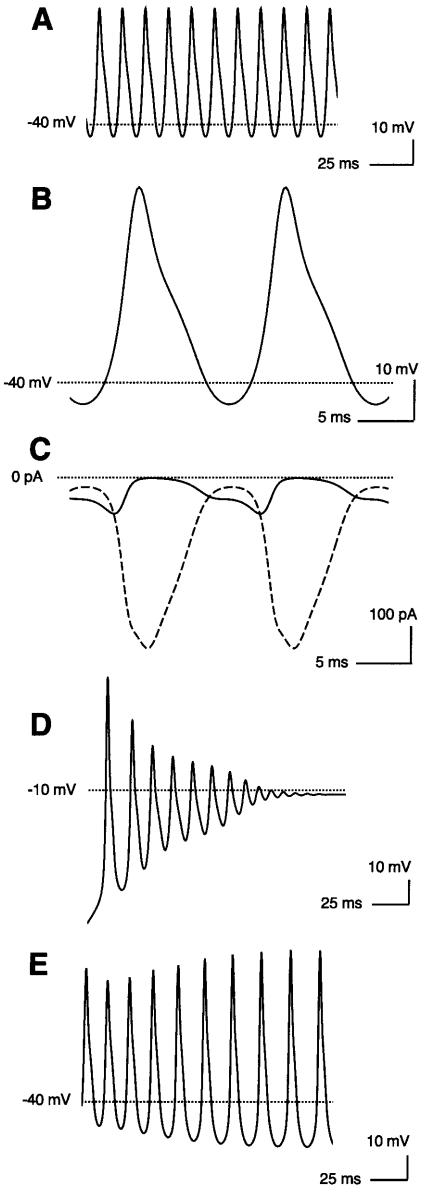

FIGURE 9 Spontaneous activity under partial blockade of potassium channels. (*A*) Simulated spontaneous activity with conductances of $I_{K,F}$ and $I_{K,S}$ set at 65% of their control values. The simulation was started with the membrane potential of the cell set at −70 mV and reached a steady firing rate after ~100 ms. (*B*) Enlarged view of the low-amplitude, broad-action potentials produced under simulated blockade of the potassium channels. (*C*) Simulated sodium currents during an action potential. $I_{Na,T}$ is represented by the solid line and $I_{Na,P}$ by the dashed line. $I_{Na,P}$ is the larger of the two except for a brief period during the interspike interval. (D) Simulated spontaneous activity with conductances of $I_{K,F}$ and $I_{K,S}$ set at 63% of their control values. The membrane voltage in the model cell undergoes a series of damped oscillations until it reaches a resting membrane potential at −12 mV. The starting membrane potential of the cell was −70 mV. (*E*) Simulated spontaneous activity with conductances of $I_{K,F}$ and $I_{K,S}$ set at 67% of their control values. The simulation was started with the membrane potential set at −45 mV to better demonstrate the oscillations leading to the steady-state behavior; after 100 msec, the action potentials were very similar to those under control conditions.

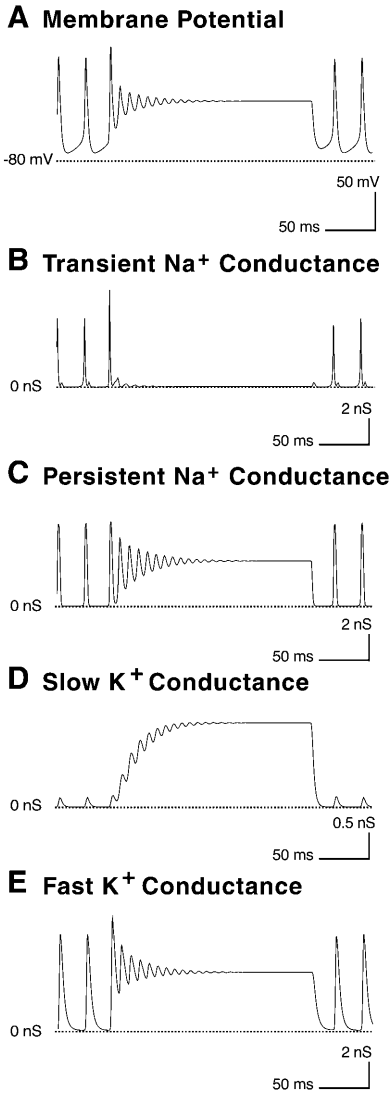

FIGURE 10 Response of the model DA cell to prolonged injection of depolarizing current, beginning 50 msec from the start of the figure. (*A*) After the depolarization, the model DA cell fires one large action potential, and then the membrane potential undergoes a series of damped oscillations. The membrane potential reaches a steady-state value of −16 mV. (*B*) After the first action potential, the transient sodium conductance becomes inactivated by the depolarization. (*C*) The persistent sodium conductance undergoes a series of damped oscillations like the membrane potential, reaching a steady-state value of 3.5 nS. (*D*) The slow potassium conductance cannot follow the rapid oscillations in the membrane potential and increases in amplitude, reaching a steady state at 1.3 nS. (*E*) The fast potassium conductance also undergoes damped oscillations, reaching a steady-state value at 5.5 nS.

TTX (Solessio et al., 2002). In a reduced model of the DA cell based on our voltage-clamp data, the spontaneous action potentials were initiated by I_{NaT}, despite the presence of a small potassium current at the most hyperpolarized membrane potential, −70 mV. The potassium current increased in amplitude slightly as the model DA cell gradually depolarized, but I_{NaP} was activated. By the peak

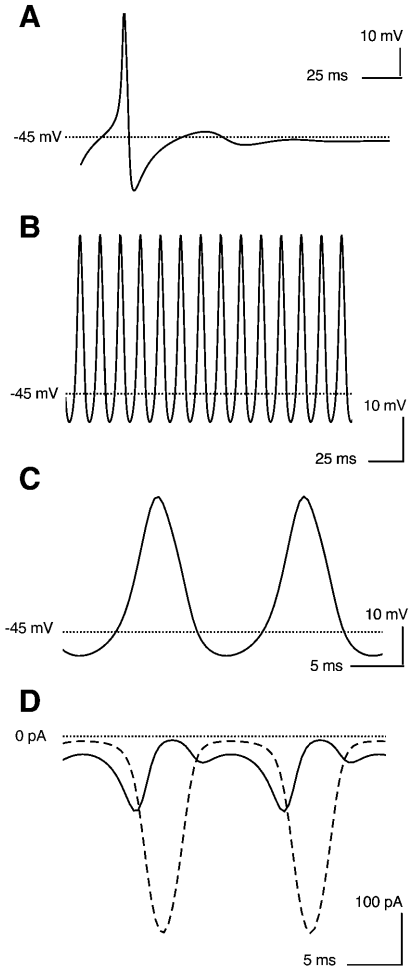

FIGURE 11 Spontaneous activity with simulated tonic inhibition. (*A*) Behavior of the model DA cell with tonic inhibition in the absence of $I_{Na,T}$. Leak conductance of the cell was set at 2 nS (as compared to 0.4 nS under control conditions), and conductance of $I_{Na,T}$ was set at 0. The cell fired once and then reached a resting potential of −46 mV. (*B*) Behavior of the model DA cell with both sodium currents and tonic inhibition. Leak conductance of the cell was set at 5 nS. The cell was still spontaneously active; it hyperpolarized to −55 mV between spikes and reached +4 mV at maximal depolarization. (*C*) Enlarged view of the action potentials produced under simulated tonic inhibition of the model DA cell. (*D*) Simulated sodium currents during an action potential under tonic inhibition. $I_{Na,T}$ is represented by the solid line and $I_{Na,P}$ by the dashed line. $I_{Na,T}$ plays a large role during the interspike interval and the rising phase of the action potential.

of the action potential, I_{NaT} was almost completely inactivated; virtually all the inward current was carried by I_{NaP}. The potassium currents were also maximal at the peak of the action potential and repolarized the cell. I_{NaT} appeared to make a small contribution during the falling phase of the action potential, but this may not be realistic. I_{NaT} reactivated briefly as it passed through an open state during recovery from inactivation, according to the classic Hodgkin-Huxley scheme. However, more recent kinetic schemes for sodium currents, where the channel recovers from inactivation without passing through the open state, do not show the transient in the falling phase (Kuo and Bean, 1994). When the model DA cell was hyperpolarized, as it would be with tonic GABAergic input, I_{NaT} made a larger contribution (Fig. 11). The behavior of the cells when I_{NaT} is blocked suggests a possible explanation for the resting potential of −46 mV in isolated mouse DA cells that were not spontaneously active (Gustincich et al., 1997; Feigenspan et al., 1998).

Only the persistent component of the sodium current was necessary to generate the spontaneous subthreshold potentials and action potentials in the model DA cells (Fig. 8). The transient component made its major contribution during the interspike interval. In these respects, the two components had essentially the opposite roles as in typical neurons (reviewed by Crill, 1996 and by Ogata and Ohishi, 2002). For example, in spinal motoneurons, a fast persistent sodium current is essential for initiating action potentials (Lee and Heckman, 2001), and in the brainstem, persistent currents generate bursting pacemaker behavior in a subset of inspiratory neurons (Del Negro et al., 2002).

The sodium current was also different from those described previously in amacrine cells from goldfish, rabbit, and rat retinas. In the isolated retina and retinal slices from goldfish, persistent sodium currents are present in nearly all amacrine cells, including some that lack transient sodium currents. The persistent sodium current is activated at −50 mV, ~10 mV positive to the resting membrane potential, and it makes a major contribution to the light responses, boosting the excitatory postsynaptic potentials and increasing the sensitivity of the amacrine cells to light stimuli (Watanabe et al., 2000). The same current appears to be present in amacrine cells of the rabbit retina because tetrodotoxin reduces the amplitude of slow potentials generated by light in these cells (Bloomfield, 1996). A persistent sodium current that amplifies graded, depolarizing potentials has also been described in cultured, GABAergic rat amacrine cells. This persistent current is relatively large, comprising ~5% of the peak sodium current (Koizumi et al., 2001).

The key difference between the DA cell and other amacrine cells is that the persistent component of the sodium current in the DA cells activates at more depolarized potentials than the transient component. In goldfish amacrine cells and in rat amacrine cells, the persistent component of the sodium current activates at the same potential or at more hyperpolarized potentials than the transient component of the current (Watanabe et al., 2000; Koizumi et al., 2001). The persistent component of the sodium current in DA cells and in goldfish amacrine cells activate at similar membrane potentials, ~−60 mV, and both are half-maximal at ~−20 mV. The major difference, therefore, between the DA cell and goldfish amacrine cells is that the transient component of the sodium current activates at substantially more hyperpolarized potentials in the DA cells. In rat amacrine cells, however, the situation is reversed. In these cells, the transient component is half-maximal at ~−27 mV (Koizumi et al., 2001), comparable to the value for $I_{Na,T}$ in the model DA

cells, but the activation of the persistent component is at ~−37 mV, much more hyperpolarized than for the persistent current in DA cells. In AII amacrine cells from rat retina, the sodium current activates at even more hyperpolarized potentials; in these cells, the threshold ranges from −65 to −60 mV (Boos et al., 1993). Thus, both components of the sodium current in the DA cell activate within the range described previously for sodium currents in retinal amacrine cells.

The persistent component and the transient component of the sodium current may be carried by distinct sets of channels, or else the persistent current may be the result of a change in gating modes that a subpopulation of channels undergoes at more depolarized potentials (Crill, 1996; Agrawal et al., 2001; Magistretti and Alonso, 2002; Clay, 2003). A third possibility is that a single population of channels mediates both transient and persistent behavior (Taddese and Bean, 2002). For example, the $Na_V1.6$ sodium channel (formerly Scn8a or NaCh6), which has been studied extensively in many different areas of the central nervous system, has been found to mediate resurgent and persistent sodium currents as well as transient sodium currents (Smith et al., 1998; Dietrich et al., 1998; Pan and Beam, 1999). $Na_V1.6$ is responsible for TTX-sensitive spontaneous activity in rat cerebellar Purkinje cells (Raman and Bean, 1997), and it has also been studied in mouse spinal neurons (Pan and Beam, 1999) and *Xenopus* oocytes (Dietrich et al., 1998). In voltage-clamp studies of $Na_V1.6$ channels expressed in *Xenopus* oocytes, the persistent current increased as a fraction of peak current with increasing depolarization in voltage-clamp experiments, just as we found in the DA cells. In these cells, the transient component activated at more depolarized voltages than in DA cells, however. The current reached half-activation at −9 mV in cells where only an α subunit was expressed and at −17 mV in cells where $\beta1$ and $\beta2$ subunits were also expressed (Smith et al., 1998). In rat cerebellar Purkinje cells, the transient current mediated by $Na_V1.6$ also reaches half activation at ~−33 mV (Raman and Bean, 1999), the same value we found for DA cells.

The first study of spontaneous activity in DA cells relied on subtraction of voltage-clamp records in the presence and absence of TTX to isolate the sodium current (Feigenspan et al., 1998). However, more recent work suggests that different components of the sodium current in the DA cell may have different TTX sensitivities (Feigenspan et al., 2001). This result may explain why the TTX subtraction protocol identified only a single component of the sodium current in the DA cells. Because the different components of the sodium current are differentially sensitive to TTX, it may be possible to separate the components, at least partially, in future experiments.

Studies of the effect of second messengers on the sodium current in DA cells are also likely to be important in characterizing its components. In experiments on fish retinal ganglion cells, elevation of cytoplasmic adenosine 3′,5′ monophosphate reduces the amplitude of the rapidly inactivating component of the sodium current and augments the slowly inactivating component (Hidaka and Ishida, 1995). Similar phosphorylation-dependent modulation of sodium channels also has been reported in neocortical neurons. Activation of D1-like dopamine receptors reduces the transient sodium current through the protein kinase A (PKA) pathway, but it has a much smaller effect on the persistent current in the same cells. One possible explanation for this difference is that $Na_V1.6$ channels make a large contribution to the persistent current in cortical pyramidal neurons, and $Na_V1.6$ is only weakly modulated by PKA because it lacks the major PKA phosphorylation site (reviewed in Cantrell and Caterall, 2001).

In voltage-clamp experiments that are not reported here, the sodium current in DA cells was best fit with a three-component model, including: a rapidly inactivating component, a more slowly inactivating component, and a component that does not inactivate at all (Feigenspan et al., 2001). Some inactivation of the persistent sodium current has been reported in goldfish amacrine cells, as well (Watanabe et al., 2000). The decay of sodium currents in goldfish retinal ganglion cells is also best fit by a three-term expression of the form:

$$I_{Na} = A_{fast}\exp(-t/\tau_{fast}) + A_{slow}\exp(-t/\tau_{slow}) + C \qquad (5)$$

(Hidaka and Ishida, 1998). However, we used a two-component model of the sodium current in the DA cells because we were unable to constrain a three-component model with the available data and because we were able to duplicate all the key properties of spontaneous activity in the DA cell with only our two-component model.

Four voltage-dependent conductances in addition to those already in the model have been described in the mouse DA cells. These other channels are not required for the spontaneous activity of DA cells, but they have a number of other, important functions (Feigenspan, et al., 1998). There is a high-threshold calcium channel, which contributes slightly to the amplitude of the spikes but does not influence the spike frequency. There is a calcium-dependent potassium conductance which contributes to repolarization of the DA cells and slows the rate of spontaneous firing slightly. There is also an A-type potassium current that produces an afterhyperpolarization and slows the rate of spontaneous firing (Feigenspan et al., 1998). In the model DA cell, $I_{K,S}$ played a major role in creating the depolarizing block, and in this respect it is similar to a slow potassium conductance in octopus cells of the cochlear nucleus (Cai et al., 1997, 2000). Approximately four times as much current was required to produce depolarizing block in our model as in mouse DA cells. It is possible that the depolarizing block in mouse DA cells is produced by an interaction between calcium and potassium conductances that were not modeled. During prolonged stimulation, there may be insufficient time for calcium that enters to be buffered or extruded, and this might increase the potassium conduc-

tance. Another possibility is that a slow inactivation process in the sodium current that was not included in the model may account for the depolarizing block.

The work was supported by the National Institute of Neurological Disorders and Stroke program (project grant NS38310).

REFERENCES

Agrawal, N., B. N. Hamam, J. Magistretti, A. Alonso, and D. S. Ragsdale. 2001. Persistent sodium channel activity mediates subthreshold membrane potential oscillations and low-threshold spikes in rat entorhinal cortex layer V neurons. *Neuroscience.* 102:53–64.

Bloomfield, S. A. 1996. Effect of spike blockade on the receptive field size of amacrine and ganglion cells in the rabbit retina. *J. Neurophysiol.* 75:1878–1893.

Boos, R., H. Schneider, and H. Wassle. 1993. Voltage- and transmitter-gated currents of all-amacrine cells in a slice preparation of the rat retina. *J. Neurosci.* 13:2874–2888.

Cai, Y., J. McGee, and E. J. Walsh. 2000. Contributions of ion conductances to the onset responses of octopus cells in the ventral cochlear nucleus: Simulation results. *J. Neurophysiol.* 83:301–314.

Cai, Y., E. J. Walsh, and J. McGee. 1997. Mechanisms of onset responses in octopus cells in the cochlear nuclei: Implications of a model. *J. Neurophysiol.* 78:872–883.

Cantrell, A. R., and W. A. Caterall. 2001. Neuromodulation of Na^+ channels: an unexpected form of cellular plasticity. *Nat. Rev. Neurosci.* 2:397–407.

Clay, J. R. 2003. On the persistent sodium current in squid giant axons. *J. Neurophysiol.* 89:640–644.

Crill, W. E. 1996. Persistent sodium current in mammalian central neurons. *Annu. Rev. Physiol.* 58:349–362.

Del Negro, C. A., N. Koshiya, R. J. Butera, Jr., and J. C. Smith. 2002. Persistent sodium current, membrane properties and bursting behavior of pre-botzinger complex inspiratory neurons in vitro. *J. Neurophysiol.* 88:2242–2250.

Dietrich, P. S., J. G. McGivern, S. G. Delgado, B. D. Koch, R. M. Eglen, J. C. Hunter, and L. Sangameswaran. 1998. Functional analysis of a voltage-gated sodium channel and its splice variant from rat dorsal root ganglia. *J. Neurochem.* 70:2262–2272.

Feigenspan, A., S. Gustincich, B. P. Bean, and E. Raviola. 1998. Spontaneous activity of solitary dopaminergic cells of the retina. *J. Neurosci.* 18:6776–6789.

Feigenspan, A., S. Gustincich, and E. Raviola. 2001. Diversity of voltage gated sodium channels in retinal dopaminergic neurons. *Invest. Ophthalmol. Vis. Sci.* 42:S674.

Gustincich, S., A. Feigenspan, D. K. Wu, L. J. Koopman, and E. Raviola. 1997. Control of dopamine release in the retina: a transgenic approach to neural networks. *Neuron.* 18:723–736.

Hidaka, S., and A. T. Ishida. 1995. Intracellular modulation of sodium channels in goldfish retinal ganglion cells. *Invest. Ophthalmol. Vis. Sci.* 36:623.

Hidaka, S., and A. T. Ishida. 1998. Voltage-gated Na+ current availability after step- and spike-shaped conditioning depolarizations of retinal ganglion cells. *Pflugers Arch.* 436:497–508.

Hille, B. 1992. Ion Channels of Excitable Membranes, 2nd ed. Sinauer Associates, Sunderland, MA.

Hodgkin, A. L., and A. F. Huxley. 1952. The dual effect of membrane potential on sodium conductance in the giant axon of *Loligo*. *J. Physiol. (Lond.).* 116:497–506.

Kamp, C. W., and W. W. Morgan. 1981. GABA antagonists enhance dopamine turnover in the rat retina in vivo. *Eur. J. Pharmacol.* 69:273–279.

Koizumi, A., S. I. Watanabe, and A. Kaneko. 2001. Persistent Na^+ current and Ca^{2+} current boost graded depolarization of rat retinal amacrine cells in culture. *J. Neurophysiol.* 86:1006–1016.

Kuo, C. C., and B. P. Bean. 1994. Na^+ channels must deactivate to recover from inactivation. *Neuron.* 12:819–829.

Lee, R. H., and C. J. Heckman. 2001. Essential role of a fast persistent inward current in action potential initiation and control of rhythmic firing. *J. Neurophysiol.* 85:472–475.

Li, L., and J. E. Dowling. 2000. Effects of dopamine depletion on visual sensitivity of zebra fish. *J. Neurosci.* 20:1893–1903.

Magistretti, J., and A. Alonso. 2002. Fine gating properties of channels responsible for persistent sodium current generation in entorhinal cortex neurons. *J. Gen. Physiol.* 120:855–873.

Marshburn, P. D., and P. M. Iuvone. 1981. The role of GABA in the regulation of the dopamine/tyrosine hydroxylase-containing neurons of the rat retina. *Brain Res.* 214:335–347.

Marshak, D. W. 2001. Synaptic inputs to dopaminergic neurons in mammalian retinas. *In* Concepts and Challenges in Retinal Biology: A Tribute to John E. Dowling. H. Kolb, H. Ripps and S. Wu, editors. Elsevier, Amsterdam. 83–91.

O'Connor, P., S. J. Dorison, K. J. Watling, and J. E. Dowling. 1986. Factors affecting release of ^{3}H-dopamine from perfused carp retina. *J. Neurosci.* 6:1857–1865.

Ogata, N., and Y. Ohishi. 2002. Molecular diversity of structure and function of the voltage-gated Na+ channels. *Jpn. J. Pharmacol.* 88:365–377.

Pan, F., and K. G. Beam. 1999. The absence of resurgent sodium current in mouse spinal neurons. *Brain Res.* 849:162–168.

Raman, I. M., and B. P. Bean. 1997. Resurgent sodium current and action potential formation in dissociated cerebellar Purkinje neurons. *J. Neurosci.* 17:4517–4526.

Raman, I. M., and B. P. Bean. 1999. Ionic currents underlying spontaneous action potentials in isolated cerebellar Purkinje neurons. *J. Neurosci.* 19:1663–1674.

Seutin, V., L. Massotte, M. F. Renette, and A. Dresse. 2001. Evidence for a modulatory role of I_h on the firing of a subgroup of midbrain dopamine neurons. *Neuroreport.* 12:255–258.

Smith, M. R., R. D. Smith, N. W. Plummer, M. H. Meisler, and A. L. Goldin. 1998. Functional analysis of the mouse Scn8a sodium channel. *J. Neurosci.* 18:6093–6102.

Solessio, E., J. Vigh, N. Cuenca, K. Rapp, and E. M. Lasater. 2002. Membrane properties of an unusual intrinsically oscillating, wide-field teleost retinal amacrine cell. *J. Physiol.* 544:831–847.

Taddese, A., and B. P. Bean. 2002. Subthreshold sodium current from rapidly inactivating sodium channels drives spontaneous firing of tubero mammillary neurons. *Neuron.* 33:587–600.

Watanabe, S. I., S. Hiromasa, A. Koizumi, T. Takayanagi, and A. Kaneko. 2000. Tetrodotoxin sensitive persistent current boosts the depolarization of retinal amacrine cells in goldfish. *Neurosci. Lett.* 278:97–100.

Wolfart, J., H. Neuhoff, O. Franz, and J. Roeper. 2001. Differential expression of the small-conductance, calcium-activated potassium channel SK3 is critical for pacemaker control in dopaminergic midbrain neurons. *J. Neurosci.* 21:3443–3456.

Ziv, I., D. A. Baxter, and J. H. Byrne. 1994. Simulator for neural networks and action potentials: description and application. *J. Neurophysiol.* 71:294–308.